Tuning the far-field superlens: from UV to visible

Yi Xiong, Zhaowei Liu, Stéphane Durant, Hyesog Lee, Cheng Sun, and Xiang Zhang*

5130 Etcheverry Hall, NSF Nanoscale Science and Engineering Center (NSEC),
University of California, at Berkeley, Berkeley, California 94720
*xiang@berkeley.edu

http://xlab.me.berkeley.edu

Abstract: A far-field optical superlens, which is able to form sub-diffraction-limited images in the far field at UV wavelength, was recently demonstrated. In current work we present two methods to tune the working wavelength from UV to visible by tuning either the permittivity of the surrounding medium or that of the metal. A practical design is provided for each method. The tunable far-field superlens enables possible applications of the far-field superlens in sub-diffraction-limited imaging and sensing over a wide range of wavelength.

©2007 Optical Society of America

OCIS codes: (180.0180) Microscopy; (240.6680) Surface Plasmons.

References and links

1. V. G. Veselago, "The electromagnetics of substances with simultaneously negative ε and μ," Sov. Phys. Usp. **10**, 509-514 (1968).
2. J. B. Pendry, "Negative refraction makes a perfect lens," Phys. Rev. Lett. **85**, 3966-3969 (2000).
3. V. A. Podolskiy, A. K. Sarychev, and V. M. Shalaev, "Plasmon modes and negative refraction in metal nanowire composites," Opt. Express **11**, 735-745 (2003).
4. T. J. Yen, W. J. Padilla, N. Fang, D. C. Vier, D. R. Smith, J. B. Pendry, D. N. Basov, and X. Zhang, "Terahertz magnetic response from artificial materials," Science **303**, 1494-1496 (2004).
5. S. Linden, C. Enkrich, M. Wegener, J. Zhou, T. Koschny, and C. M. Soukoulis, "Magnetic response of metamaterials at 100 Terahertz," Science **306**, 1351-1353 (2004).
6. S. Zhang, W. Fan, B. K. Minhas, A. Frauenglass, K. J. Malloy, and S. R. J. Brueck, "Midinfrared resonant magnetic nanostructures exhibiting a negative permeability," Phys. Rev. Lett. **94**, 037402 (2005).
7. D. R. Smith, D. Schurig, M. Rosenbluth, S. Schultz, S. A. Ramakrishna, and J. B. Pendry, "Limitations on subdiffraction imaging with a negative refractive index slab," Appl. Phys. Lett. **82**, 1506-1508 (2003).
8. N. Fang and X. Zhang, "Imaging properties of a metamaterial superlens," Appl. Phys. Lett. **82**, 161-163 (2003).
9. R. J. Blaikie and S. J. McNab, "Simulation study of 'perfect lenses' for near-field optical nanolithography," Microelectron. Eng. **61-62**, 97-103 (2002).
10. N. Fang, H. Lee, C. Sun, and X. Zhang, "Sub-diffraction-limited optical imaging with a silver superlens," Science **308**, 534-537 (2005).
11. H. Lee, Y. Xiong, N. Fang, W. Srituravanich, S. Durant, M. Ambati, C. Sun, and X. Zhang, "Realization of optical superlens imaging below the diffraction limit," New J. Phys. **7**, 255 (2005).
12. D. Melville and R. Blaikie, "Super-resolution imaging through a planar silver layer," Opt. Express **13**, 2127-2134 (2005).
13. V. A. Podolskiy and E. E. Narimanov, "Near-sighted superlens," Opt. Lett. **30**, 75-77 (2005).
14. S. Durant, Z. Liu, J. M. Steele, and X. Zhang, "Theory of the transmission properties of an optical far-field superlens for imaging beyond the diffraction limit," J. Opt. Soc. Am. B **23**, 2383-2392 (2006).
15. Z. Liu, S. Durant, H. Lee, Y. Pikus, N. Fang, Y. Xiong, C. Sun, and X. Zhang, "Far-field optical superlens," Nano Lett. **7**, 403-408 (2007).
16. W. Cai, D. A Genov, and V. M. Shalaev, "Superlens based on metal-dielectric composite," Phys. Rev. B **72**, 193101 (2005).
17. M. G. Moharam, E. B. Grann, D. A. Pommet, and T. K. Gaylord, "Formulation for stable and efficient implementation of the rigorous coupled-wave analysis of binary gratings," J. Opt. Soc. Am. A **12**, 1068-1076 (1995).
18. M. G. Moharam, D. A. Pommet, E. B. Grann, and T. K. Gaylord, "Stable implementation of the rigorous coupled-wave analysis for surface-relief gratings - enhanced transmittance matrix approach," J. Opt. Soc. Am. A **12**, 1077-1986 (1995).

19. M. J. Weber, *Handbook of optical materials* (CRC Press, Boca Raton, Fla., 2003).
20. P. B Johnson and R. W. Christy, "Optical constants of the noble metals," Phys. Rev. B **6**, 4370-4379 (1972).
21. D. A. G. Bruggeman, "Calculation of various physics constants in heterogeneous substances," Annu. Phys. **24**, 636-664 (1935).

1. Introduction

The imaging resolution of conventional optical microscopes is limited to half of the illumination light wavelength because the scattered evanescent waves from the object, which carry the information of features smaller than half wavelength, can not reach the image plane in the far field. This resolution limit is commonly called diffraction limit. Recently, Pendry predicted that a slab of flat left-handed material (LHM) as first termed by Veselago [1], a material with both negative permittivity and negative permeability, could not only focus propagating waves, but also enhance evanescent waves [2]. In other words, all propagating waves and evanescent waves scattered from the object are present at the propagating waves' focus plane, which results in a perfect image. Despite the remarkable progresses on the realization of the LHM towards high frequency [3-6], it is yet challenging to provide optical LHM for practical use. Alternatively, a slab of material with only negative permittivity, usually termed as superlens, can be used to enhance evanescent waves and form sub-diffraction-limited images for p-polarization [2]. Low loss noble metals such as silver therefore become natural candidates of superlens at optical frequency. Numerical [2, 7-9] and experimental [10-12] studies have already shown that a thin silver slab indeed greatly improves the imaging resolution. Although the superlensing mechanism provides a new avenue for nanoscale optical imaging, it was pointed out that the superlens could only produce sub-diffraction-limited images in the near field [13]. This is a major drawback compared to conventional lenses which can be easily used in far-field microscopy. An important progress toward far-field optical superlens microscopy was recently reported [14, 15], in which a sub-wavelength silver grating is placed above a silver slab superlens. The evanescent waves scattered from the object are firstly enhanced by the thin silver slab and then are converted into propagating waves by the sub-wavelength silver grating. With proper design of the silver film and the grating, one can form a unique image with sub-diffraction-limited resolution in the far field [14]. In contrast with the conventional superlens (we call it near-field superlens [NSL] from now on) with near-field imaging limitation, this new device was named as the far-field superlens (FSL).

In order to achieve sub-diffraction-limited imaging resolution, the FSL has to support high transmission efficiency over a broad evanescent wavevector band which is realized by surface plasmon resonance excitation at condition $|\varepsilon_m| \approx \varepsilon_d$ [14, 15]. ε_m and ε_d are permittivities for metal and dielectric, respectively. Therefore, the properties of the materials, which determine the surface plasmon mode, will eventually determine the working wavelength of a FSL. For instance, considering a FSL made of silver surrounded with glass, the working wavelength is in the near-UV [14]. In this paper, we provide two methods to tune the working wavelength of a FSL from UV to visible range which enables more applications. The first approach is to use available non-absorbing dielectric material with high permittivity as the surrounding medium. The second approach is to modify the effective permittivity of the metal by mixing it with dielectric, as it was shown for the case of a NSL [16]. This paper is organized as following. In section 2, we will explain the FSL theory and the procedure of designing a FSL. Then it is straightforward to understand the principles of tuning the working wavelength of the FSL. In section 3 and section 4, we will discuss the two methods with examples. Section 5 is the conclusion.

2. Principle of tuning the working wavelength of the far-field superlens

The FSL is composed of a silver slab and a sub-wavelength grating. The silver slab of the FSL enhances the evanescent waves and the sub-wavelength grating of the FSL converts the enhanced evanescent waves into the propagating waves. To ensure the imaging functionality

of a FSL, the conversion of evanescent waves to propagating waves has to be one-to-one so that the high resolution information of the object (evanescent waves) can be retrieved from the propagating wave detections. The following is the detailed explanation of the one-to-one conversion. In Fourier space, the propagating waves have tangential wavevector $k_x \in [0, nk_0]$ as shown in blue in Fig. 1 (band $[-nk_0, 0]$ is symmetric to band $[0, nk_0]$, so only band $[0, nk_0]$ is considered here), where n is the refractive index of the surrounding medium, $k_0 = 2\pi / \lambda$, λ is the working wavelength (in free space) of the FSL, and Λ is period of the sub-wavelength grating. The propagating waves after the FSL have three diffractive origins: the 0 order, -1 order, and +1 order diffraction (The higher orders are ignored because of the small diffraction efficiency [14]) of the FSL with incident wavevectors within $[0, nk_0]$ (blue band), $[2\pi/\Lambda, 2\pi/\Lambda + nk_0]$ (yellow band), and $[-2\pi/\Lambda, -2\pi/\Lambda + nk_0]$ (orange band) respectively (The incident waves are the scattering waves from the object at the plane immediately before the FSL [plane II in Fig. 2]). The FSL is designed in a way that the propagating part of the diffracted waves after the FSL mainly comes from the -1 order diffraction of the incident waves within the yellow band. Then by measuring the spectrum of the propagating waves after the FSL, the information of the incident waves within the yellow band is retrieved. The information of the incident waves within the blue band can be obtained by a reflection mode of a conventional optical microscope, or using a different polarization [15]. As a result, the information of the incident waves within the blue and yellow band can be obtained for reconstruction of sub-diffraction-limited images. However the information in the band $[nk_0, 2\pi/\Lambda]$ (between the blue and yellow band) is missed. Obviously it is desirable to reduce this missing band.
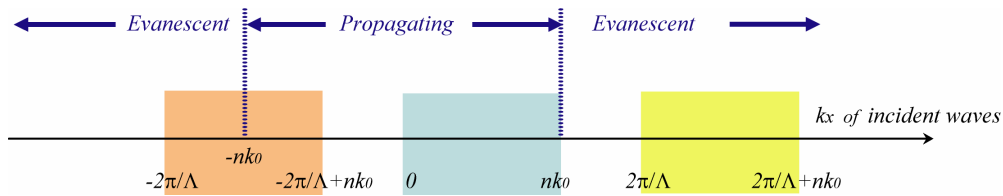

Fig. 1. Three contributions to the propagating waves after the FSL

Suppose we choose a working wavelength λ_{FSL}. We can design a FSL working at λ_{FSL} by two steps. The enhancement of evanescent waves by the silver slab in a FSL is the most essential factor in the FSL functionality. Therefore, in the first step, we use a NSL as a rough design guidance to determine the surrounding dielectric and the thickness of the silver slab in a FSL. The surrounding dielectric is selected so that the working wavelength of the NSL λ_{NSL} is close to λ_{FSL}. The thickness of the superlens is optimized so that the transmission coefficient is large over a broad tangential wave-vector range. Ideally the transmission coefficient is large for incident waves within $[nk_0, 2nk_0]$ but is small for incident waves within $[0, nk_0]$. Refer to Fig. 3 for an example of calculated transmission coefficients of a NSL. In the second step, utilizing the parameters fixed in the first step, we add the sub-wavelength grating above the NSL and optimize the geometrical parameters of the sub-wavelength grating (period, thickness, and metal filling ratio) by best satisfying both of the following two requirements at λ_{FSL}: (1) the -1 order transfer function of the FSL is much larger than that of the +1 order and the 0 order, and (2) width of band $[nk_0, 2\pi / \Lambda]$ is minimized. The transfer functions of the FSL are defined as the wave amplitude ratio between the diffracted waves at plane I and the incident waves at plane II in Fig. 2. The transfer functions for different orders are calculated with Rigorous Coupled Wave Analysis (RCWA) [17, 18].
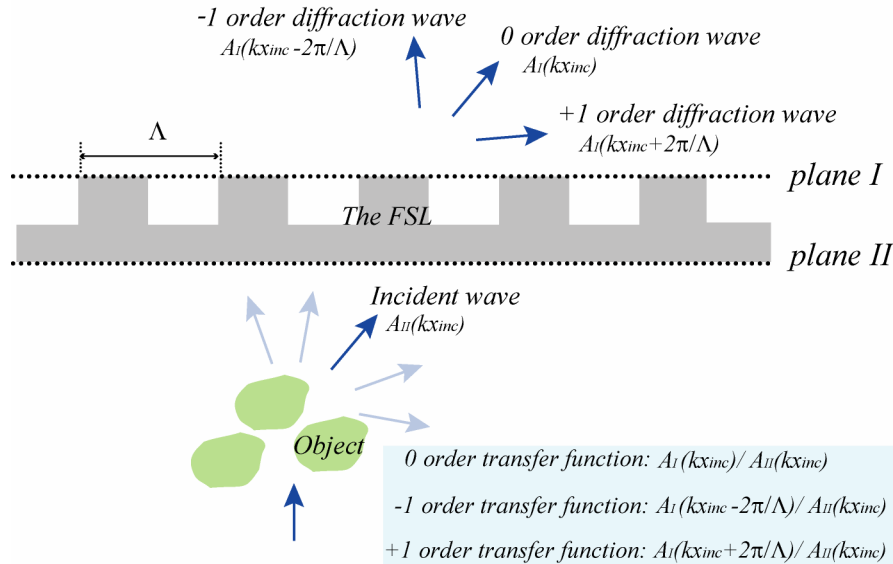
-1 order diffraction wave
$A_I(kx_{inc} -2\pi/\Lambda)$

0 order diffraction wave
$A_I(kx_{inc})$

+1 order diffraction wave
$A_I(kx_{inc}+2\pi/\Lambda)$

Λ

plane I

The FSL

plane II

Incident wave
$A_{II}(kx_{inc})$

Object

0 order transfer function: $A_I(kx_{inc})/A_{II}(kx_{inc})$

-1 order transfer function: $A_I(kx_{inc} -2\pi/\Lambda)/A_{II}(kx_{inc})$

+1 order transfer function: $A_I(kx_{inc}+2\pi/\Lambda)/A_{II}(kx_{inc})$

Fig. 2. Definitions of the transfer functions

Since λ_{FSL} is close to λ_{NSL}, considering that λ_{NSL} is determined by permittivities of metal and dielectric, it is clear that the working wavelength of the FSL can be tuned either by changing surrounding dielectric or the metal. In section 3 and section 4, we will discuss the two methods with examples.

3. Tuning the far-field superlens by changing the surrounding dielectric

As mentioned above, one way to change the working wavelength of the FSL is to change the permittivity of the surrounding dielectric. To tune the FSL working wavelength from UV to visible range, we need to increase the permittivity of the surrounding dielectric to match the permittivity of the metal $/\varepsilon_m/$ at visible range. As an example, we show how to design a FSL with working wavelength 457.9nm (one of the Argon LASER wavelengths) by selecting the GaN as the surrounding dielectric. We also show how to finalize the geometrical parameters of the FSL. The same procedure can be applied to design a FSL working at other visible wavelengths.

The permittivity of GaN is 6.24 at 440nm [19], which matches the permittivity of Ag (-6.50+0.19i) at 440nm [20]. Aiming at high enhancement factor and broad enhancement wavevector band, we calculated the transmission coefficients of a silver slab with various thicknesses embedded in GaN. Figure 3 shows the calculated transmission coefficients with an optimized silver thickness of 30nm surrounded by GaN. The wavelength is equal to 440nm which is slightly smaller than the desired FSL working wavelength 457.9nm. However, this consequence is rather favorable for the FSL design since the best working wavelength of the FSL should be moderately larger than λ_{NSL}. It is obvious from Fig. 3 that the left edge of the enhancement band reduces when the working wavelength is enlarged, which essentially reduces the missing band $[nk_0, 2\pi/\Lambda]$.

A sub-wavelength grating composed of GaN and Ag was added to the silver slab to build the FSL. Transfer functions of the FSL were calculated by RCWA with different geometrical parameters of the sub-wavelength grating at the working wavelength of the FSL 457.9nm. The period of the sub-wavelength grating was changed from 90nm to 150nm with 10nm step, the thickness from 5nm to 95nm with 5nm step, and the Ag filling ratio of grating from 0.1 to 0.9 with 0.1 step. The final geometrical parameters of the sub-wavelength grating were chosen so

that the two requirements mentioned in section 2 were best satisfied. Figure 4(b) shows the final configuration of the FSL (the grating period is 120nm, the grating thickness is 40nm and the filling ratio of Ag is 0.3).
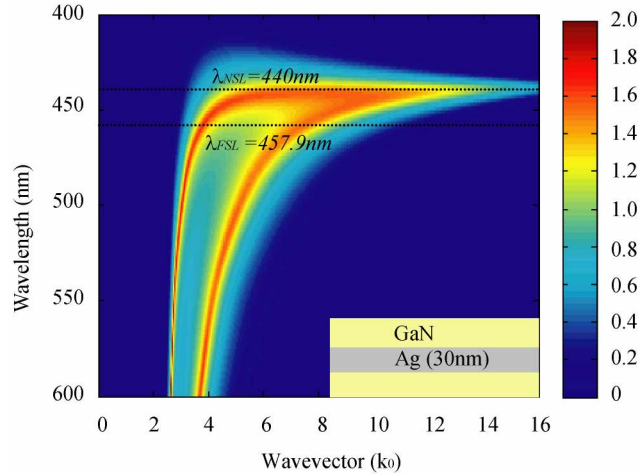

Fig. 3. Calculated transmission coefficients (in logarithm scale) of a silver slab surrounded by GaN. Insets show the schematic geometry of the sample configuration.

Figure 4(a) shows the transfer functions of such a GaN-Ag FSL at 457.9nm. The transfer functions plotted in Fig. 4(a) only show the bands which are possible to be coupled into the propagating band. Considering the refractive index of GaN is 2.48 at this wavelength and the grating vector is $3.82k_0$, the propagating band of the diffracted waves after the FSL has three possible origins: the 0, -1 and +1 order diffraction waves of incident waves with $kx_{inc} \in [0, 2.48k_0]$, $kx_{inc} \in [3.82k_0, 6.29k_0]$, and $kx_{inc} \in [-3.82k_0, -1.34k_0]$, respectively [see the black, blue and red curves in Fig.4(a)]. It can be seen that the -1 order transfer function of incident waves is about one-order larger than that of the rest two. Therefore, the dominance of the -1 order diffraction is satisfied, as required by the FSL microscopy. The highest retrievable wavevector of this FSL thus goes up to $6.29k_0$. Comparing with the highest propagating wavevector in the host dielectric (i.e. $2.48k_0$), about 2.5 fold improvement has been achieved.

Figure 4(c) compares the diffraction-limited image of a sub-diffraction-limited object and the image reconstructed by the FSL. The object, located at the plane immediately before the FSL (plane II in Fig. 2), is a two-line source with 30nm line-width and 40nm separation. The H field is 1 at the two-line position and 0 elsewhere. Without the FSL, only the information in the propagating band $[-2.48k_0, 2.48k_0]$ can be collected in the far-field, which results in a diffraction-limited image [blue curve in Fig. 4(c)]. In the diffraction-limited image, two lines are indistinguishable, which is expected as the separation of the two lines is sub-diffraction-limited. With the FSL, the information in the bands $[-6.29k_0, -3.82k_0]U[-2.48k_0, 2.48k_0]U[3.82k_0, 6.29k_0]$ can be retrieved by the spectrums collected in the far field. The FSL image formed from these spectrums is shown by the red curve in Fig. 4(c) (See Ref. [14] for more details of the procedure of the FSL image reconstruction). Evidently two lines can be recognized in the FSL image.
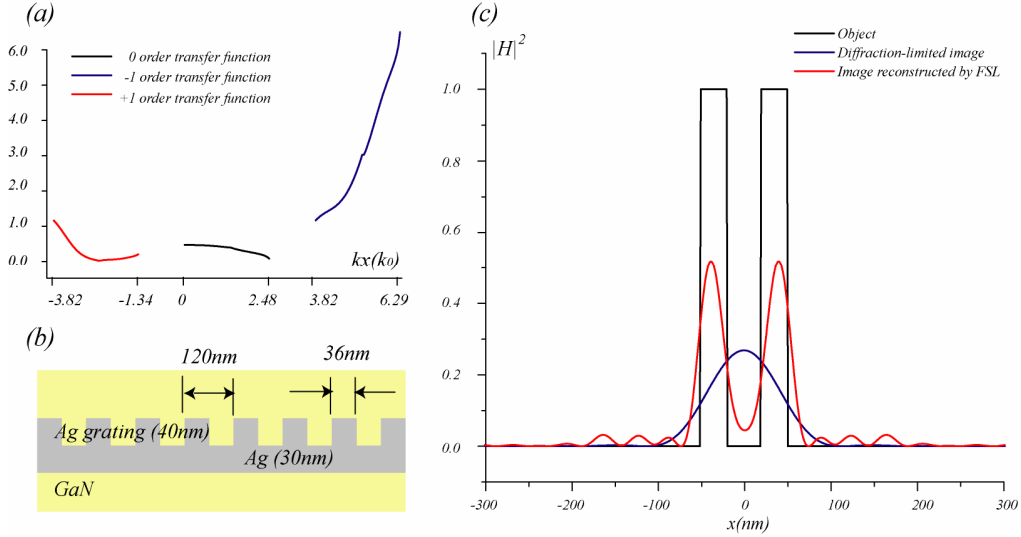
Fig. 4. (a). The transfer functions of a GaN-Ag FSL working at 457.9nm. (b). The detailed geometry of the FSL. (c). The image reconstructed by the FSL and conventional lens. The object is two-line source with 30nm line width and 40nm separation.

4. Tuning the far-field superlens by adjusting the effective metal permittivity

The working wavelength of the FSL can also be increased from UV to visible by decreasing the metal permittivity $|\varepsilon_m|$ to match the permittivity of the surrounding dielectric at visible range. One solution to decrease the metal permittivity $|\varepsilon_m|$ is to use the metal-dielectric composite as discussed in Ref. [16]. The metal-dielectric composite may be fabricated by using metal particle aggregates or by depositing two materials at the same time. By effective medium theory (EMT), the effective permittivity for a two-dimensional composite (metal particles with permittivity ε_m and volume filling ratio p inside dielectric with permittivity ε_d) is [21, 16]

$$\varepsilon_e = \frac{1}{2}\{(2p-1)(\varepsilon_m - \varepsilon_d) \pm \sqrt{(2p-1)^2(\varepsilon_m - \varepsilon_d)^2 + 4\varepsilon_m\varepsilon_d}\} \tag{1}$$

where the sign is chosen so that the imaginary part of ε_e is positive. The accuracy of applying EMT to metal-dielectric composite and the issue of spatial dispersion were discussed in Ref. 16. When the length scale of inhomogeneities is less than 20nm, it is valid to use EMT to obtain the resolution of $\lambda / 10$ [16].

We designed a near-field superlens by using the Ag-air composite as the metal slab and Al_2O_3 as the surrounding dielectric and targeted that the permittivity of Ag-air composite matches the permittivity of Al_2O_3 at 440nm. Here wavelength 440nm was chosen again to show that the current method can tune the working wavelength of the FSL to 457.9nm as effectively as the method in section 3. When p=0.85, the real part of the permittivity of the Ag-air composite is -3.27 (The real part of the permittivity of Ag is -6.50 at 440nm), which closely matches the permittivity of Al_2O_3 (3.17) at 440nm [19]. The imaginary part of the permittivity of the Ag-air composite is small: 0.21 at wavelength 440nm and 0.19 at wavelength 457.9nm.

Similarly, the geometrical parameters of Ag-air composite-Al_2O_3 FSL were chosen based on transfer functions calculated by RCWA. The period of the sub-wavelength grating was changed from 130nm to 210nm with 10nm step, the thickness from 20nm to 95nm with 5nm step, and the Ag filling ratio of grating from 0.1 to 0.9 with 0.1 step. The optimized

parameters are: 170nm period, 0.4 Ag filling ratio and 55nm thickness. Figure 5(a) shows the transfer functions of Ag-air composite-Al_2O_3 FSL at working wavelength 457.9nm and Fig. 5(b) shows the configuration of the FSL. Again it can be seen that the -1 transfer function of incident waves with $kx_{inc} \in [2.69k_0, 4.47k_0]$ is about one-order larger than the +1 order transfer function of incident waves with $kx_{inc} \in [-2.69k_0, -0.92k_0]$, and the 0 order transfer function of incident waves with $kx_{inc} \in [0, 1.78k_0]$. The dominance of the -1 order diffraction from this FSL design is satisfied. The highest retrievable wavevector goes up to $4.47k_0$. Figure 5(c) compares the diffraction-limited image of a sub-wavelength object and the image reconstructed by the FSL. The object, located at the plane immediately before the FSL (plane II in Fig. 2), is a two-line source with 40nm line-width and 50nm separation. The H field is 1 at the two-line position and 0 elsewhere. The two lines can be recognized in the FSL image but are indistinguishable in the diffracted-limited image.
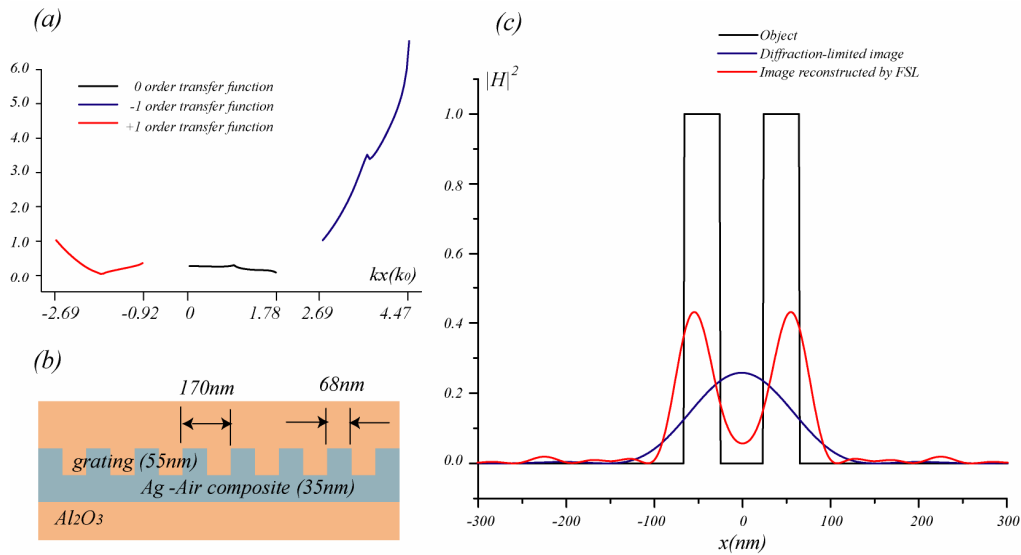

Fig. 5. (a). The transfer functions of a Ag air composite-Al_2O_3 FSL working at 457.9nm. (b). The detailed geometry of the FSL. (c) The image reconstructed by the FSL. The image reconstructed by the FSL and conventional lens. The object is two-line source with 40nm line width and 50nm separation.

As a comparison of the method in section 3 (first method) and section 4 (second method), the fabrication of the second method is more demanding. However the second method is more flexible in terms of tuning the working wavelength of the FSL because the filling ratio of the Ag in the Ag-dielectric is tunable. Of course, these two methods can always be combined.

5. Conclusions

We presented novel methods to tune the FSL working wavelength from UV to visible: increasing the permittivity of the surrounding medium or decreasing the effective metal permittivity. With practical examples, we show that both methods can design a FSL working at wavelength 457.9nm. The same procedures can be applied to tune the working wavelength of FSL to other visible wavelengths. The tunability of the FSL working wavelength enables more applications of the FSL in sub-diffraction-limit imaging. As future work, it would be of great interest to use materials with electrically tunable permittivity, such as liquid crystals, to tune the working wavelength of the FSL dynamically.

Acknowledgments